44TH TURBOMACHINERY & 31ST PUMP SYMPOSIA
HOUSTON, TEXAS | SEPTEMBER 14 – 17 2015
GEORGE R. BROWN CONVENTION CENTER

NUMERICAL PREDICTION AND EXPERIMENTAL VALIDATION OF ROTOR THERMAL INSTABILITY

Daniele Panara, L. Baldassare
GE Oil&Gas
Florence, Italy

D. Griffini, A. Mattana,
Department of Industrial Engineering
Florence, Italy

S. Panconi, E. Meli
Department of Industrial Engineering
Florence, Italy

Daniele Panara is Axial and Centrifugal Compressor Rotordynamic Senior Engineer at GE Oil&Gas. He holds a PhD in Aeronautical Engineering, a specialization in Fluid dynamics and has 11 years of experience in Numerical Simulations (CFD and Structural Dynamics)

ABSTRACT

The increasing demand of higher efficiency and increased equipment compactness is pushing the modern rotordynamic design towards higher and higher bearing peripheral speeds. Due to the increased viscous dissipation, fluid film bearings are prone to the development of rotor asymmetrical heating (de Jongh 1994) and hence thermal rotor bowing, rotor thermal imbalance and consequent synchronous vibration increase. Differential heating and synchronous rotor vibrations are directly linked leading to a complex feedback loop which can cause thermal rotor instability often referred as Morton effect (de Jongh 1994). In the present work, the stability of a rotor bearing system is numerically simulated following two different approaches: a classical linear stability approach suggested by Murphy et al. (Murphy 2009) and an iterative FEM thermo-structural-dynamic analysis. Results are compared with measurements obtained during an experimental campaign carried out at the GE oil & Gas facility in Florence on a real scale between-bearing dummy rotor. During the experiments, the rotor differential temperature at the journal bearing section has been continuously monitored via telemetry as well as rotor vibration at bearing, mid span and overhung location. For the linear stability approach, the rotor differential temperature is estimated by making use of a steady thin-film tilting pad journal bearing (TPJB) code developed at the Department of Industrial Engineering of the University of Florence while the iterative method takes advantage of an experimentally fit correlation between rotor vibration and differential rotor temperature used to couple the dynamic and thermo-structural rotor simulations.

INTRODUCTION

Since the pioneering works of Morton (Morton 1975) and Hesseborn (Hesseborn 1978) the problem of rotor thermal instability has been receiving more and more attention from both the academic and industrial community. An excellent historical excursus has been given by de Jongh (de Jongh 2008). In his 2008 paper, the synchronous rotor instability was still defined as a “not well-known rotordynamic phenomenon”. He reported the number of technical papers written on this subject over the years showing a clear upswing. In Figure 1 the de Jongh technical paper overview has been integrated with the publication from 2008 to 2015 known by the authors clearly confirming this trend also to the present days.

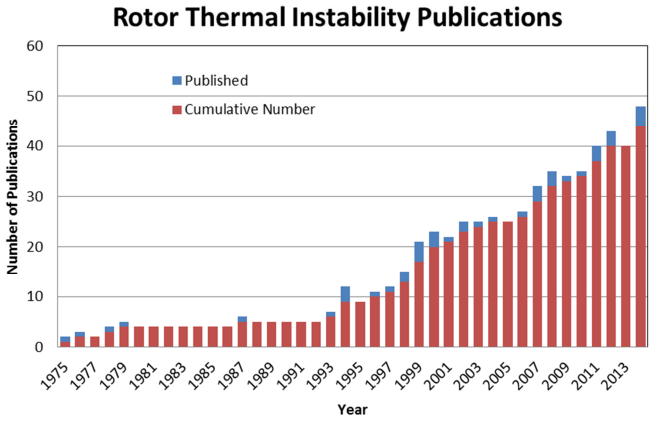

Figure 1: Rotor Thermal instability Technical Publications.

From the industrial side, an interesting fact showing the increasing attention of the turbomachinery world to the rotor thermal instability is the appearance of a dedicated chapter in the second revision of the American Petroleum Institute rotordynamic tutorial (API684 standard, paragraph 3.5.2.5: Synchronous Thermal Instability “Morton’s Effect”) (API 684 2005).This demonstrates that the rotor thermal instability is becoming more and more a technology challenge recognized by industry which solution is still under discussion in the technical community. As stated in the API standards paragraph closure:

"while synchronous thermal instability fits the classical definition of an unstable system, rotor stability codes are currently not used to predict its existence". The aim of present work is to overcome current code limitations presenting two possible prediction strategies.

In order to introduce the thermal instability phenomenon it is possible to use the API 684 words: "Research has shown that rotors supported in fluid film bearings will exhibit a non-uniform temperature distribution". This unavoidable thermal gradient is rotating with the shaft and can be explained in simple terms as follows: "one specific point on the shaft will always be on the outside of the orbit (the high spot) and will therefore be closer to the bearing wall (Figure 2). This surface will have a smaller film thickness averaged over the period of one orbit than the opposite side of the shaft" (API 684 2005).

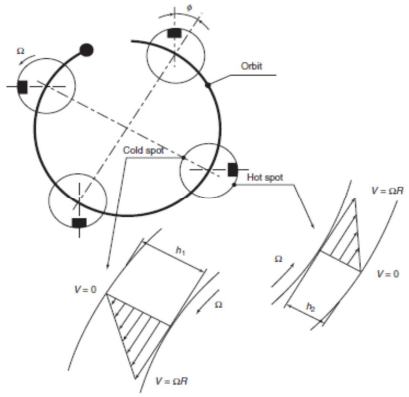

Figure 2: Differential Heating at Bearing Journal for Synchronous Forward Whirl (De Jongh and Ver Hoeven 1998, extract from API 684, 2005)

Since oil temperature is directly proportional to viscous shear, it is easy to show that oil temperature grows inversely to the oil film thickness producing a hot and cold spot on the rotating shaft. Rotating thermal gradient determines shaft thermal bending and hence rotor unbalance. If the increased thermal unbalance couples positively with vibration orbit enhancement the resulting feedback loop can drive the rotor unstable in the sense that the synchronous vibration will grow unbounded (not to be confused with sub-synchronous rotor instability).

Due to the variety of the phenomena involved, different models with different degree of complexity were proposed. In order to assess the stability of the system, three main physical aspects interconnected in a loop to each other need to be numerically/analytically or empirically defined (see Figure 3): 1) the link between thermal unbalance and rotor vibration at bearing section (here in after referred as A correlation), 2) the link between rotor vibration at bearing section and rotor differential heating (here in after referred as B correlation) and 3) the link between rotor differential heating and thermal unbalance (here in after referred as C correlation). System stability may be assessed: a) simulating with time accuracy the evolution of the complete system, b) iterating between the quasi-steady solutions of each of the above physical aspects assuming a segregation of effects and c) using some stability theory criteria or empirical evaluation of stability based on the assessment of A, B and C correlation mutual importance.

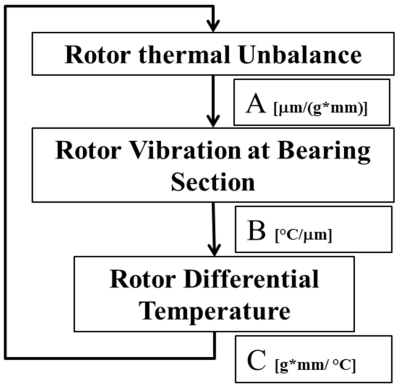

Figure 3: Scheme of Instability Phenomenon

Schmied proposed for A and C terms a beam finite element model (Schmied 1987). An equivalent of the B correlation is formulated on the base of an empirical equation proposed by Kellenberger (Kellenberger 1979) and coupled with the finite element method. The system stability could be assessed studying the overall finite element method evolution in time or on the base of the evaluation of the so called thermal eigenvalues of the finite element system solution matrix.

De Jongh and Morton (de Jong 1994) were the first to laboratory reproduce and openly publish a thermal instability field issue occurred on an offshore between-pad centrifugal compressor. They directly measured the rotor thermal gradient and explained the thermal instability assessing from theory the A and C term while the B term was evaluated through the shaft thermal gradient laboratory measurements. To assess stability, they successfully applied a control theory criterion evaluating the gain of the A, B and C coupled system in loop.

Larsson (Larsson 1997) characterized the B and C terms using an analytical formulation based on the numerical work of Ericsson (Ericsson 1980). He obtained an analytical correlation between bow and shaft vibration. He considered also the influence of shaft thermal boundary conditions assessing the influence of such terms on the analytical correlation by means of finite difference thermal calculations. The A term was evaluated using a beam finite element rotor model and everything was coupled in order to compute the overall system solving matrix eigenvalues and assess stability.

Balbahadur and Kirk (Balbahadur 2002a) approach was to characterize B by simply averaging the temperature results of a steady state bearing solver at different imposed orbital positions. The C term was determined using a simple analytical relation depending on thermal gradient and equivalent shaft overhung dimensions. A criteria for thermal instability was given comparing estimated thermal unbalance (B*C term) and

rotor weight.

Murphy and Lorenz (Murphy 2009) following the strategy used by de Jongh and Morton and the method of Kirk and Balbahadur proposed a simplified method based on linear stability theory to predict rotor thermal instability. For the evaluation of the A term a standard rotordynamic code was used.

To evaluate B and C, the same approach of Kirk and Balbahadur was used taking advantage of a standard bearing code. A, B and C can be then expressed as complex coefficients and the criterion for thermal stability is simply depending on the real part of the composition of A, B and C which should not exceed the unity. The advantage of this method is surely the simplicity which of course is paid by the approximate accuracy of the simple averaging method used to estimate the B term.

Gomiciaga and Keogh (Gomiciaga 1999) instead used CFD techniques to numerically predict rotor thermal gradients on plain bearings depending on imposed forward and backward circular rotor orbits. The Navier-Stokes fluid and energy equations were solved in a 3D cylindrical reference frame. A coordinate transformation is used to take into account the boundary motion due to the imposed vibration on a fixed time independent grid domain. Similarly, Lee and Palazzolo (Lee 2013) solved the transient thin film thermo-hydrodynamic (THD) equations together with the transient shaft heat conduction. The bearing and shaft thermal solution was then coupled with a finite element rotordynamic code in order to simulate with time accuracy the evolution of the complete system. This approach was computationally very demanding and further developed by Suh and Palazzolo (Suh 2014).

A possible computationally less demanding but still accurate approach was proposed by Childs and Saha (Childs 2012). The method needs to pre-compute the rotor thermal gradient amplitude and phase for a given set of forward and backward circular orbits with different amplitude. Starting from a first response to unbalance the code computes, for a generic elliptical orbit, the rotor thermal gradient interpolating from the pre-computed thermal table. Based on the rotor thermal gradient, the shaft thermal bowing and the induced thermal unbalance is computed and the calculations are iterated. Stability is assured when the computed orbit converges to a bounded value.

Grigorev et al. (Grigorev 2014) computed the B term solving the perturbed (oscillating) thin film Reynolds equations. A similar method was used by Ericsson (Ericsson 1980) who first derived the set of equation for the oscillating temperature, film thickness and pressure. The oscillating temperature is then used to compute the shaft bowing and the equation are coupled into a beam finite element transient rotordynamic code. Stability can be monitored looking at the time evolution of the computation or through the evaluation of the numerical stability of the solution by means of the computation of the spectral radius of the time solver numerical matrix.

For all the mentioned models, the most challenging term to be evaluated seems to be the B term. The numerical estimation of the link between rotor vibration at bearing section and rotor thermal gradient requires very demanding and time consuming simulations which accuracy remains still questionable due to the lack of accurate rotor thermal gradient measurements with the only exception of the de Jongh and Morton test campaign (de Jong 1994). This leads to the necessity for the industry to carry-out dedicated experimental test campaigns in order to validate or develop prediction models which suit their own product needs.

In the present work the simplified model proposed by Murphy and Lorenz is compared with the experimental results of a dedicated test campaign carried out at the GE oil & Gas facility in Florence on a real scale between-bearing dummy rotor. During the experiment the rotor thermal gradient at the journal bearing section has been continuously monitored via telemetry as well as rotor vibrations. The experimental results have been used to develop a correlation between vibrations and temperature which is compared with the rotor differential temperature estimation obtained by a steady thin-film tilting pad journal bearing (TPJB) code developed at the Department of Industrial Engineering of the University of Florence as explained in the following. The same correlation is used to couple the dynamic results and the thermal rotor boundary conditions of an iterative FEM analysis. The experimental results and the prediction obtained with both the simplified and the experimentally fit iterative method are compared.

EXPERIMENTAL SETUP

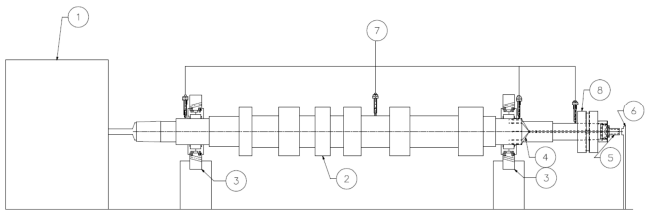

Figure 4: Experimental setup

In Figure 4 the experimental apparatus schema is reported. An electric motor (1) drives a dummy rotor (2) representative of a full scale compressor shaft. The rotor is mounted on a set of direct lubricated 5 pad journal bearings (3) with double radii pivots. Bearings were set in load on pad configuration. In order to measure the rotor differential temperature at the non-drive end bearing section, a set of eight K thermocouples equally spaced in the 360 degrees were installed few millimeters below the journal surface through a set of axial holes. The thermocouple holes were drilled axially on the vertical step surface between the journal and the successive shaft diameter reduction in the outboard bearing direction (4). The thermocouples wires are routed to the overhung shaft end through two symmetric shunt holes and a cavity drilled along the shaft axis up to the rotor non-drive end. The wires are

cabled on a ring placed into an interconnecting flange precisely fit at the shaft end and connected through electric pins to a sensor signal amplifier and a rotor antenna (5). The rotor antenna and sensor signal amplifier housing is secured to the interconnection flange and the rotor through a set of screws. The stator antenna (6) placed in front of the rotor antenna at shaft end receives the thermocouple signals and redirects the information to the evaluation unit (Figure 5). Shaft vibrations are monitored in four shaft locations: at bearing sections (drive end and non-drive end bearing), rotor mid span and shaft end (non-drive side) through Bently Nevada non-contact probes attached to an ADRE system (7). Bearing temperatures have been monitored on two pad angular positions through Pt100 thermo-resistances. The Most loaded pad (bottom pad) is equipped with two temperature probes at 25% and 75% pad arc. Another temperature probe is installed on the next downstream pad on both bearings at 75% pad arc to monitor bearing side loading. The overhung non-drive end weight can be varied by means of different idling adaptors hydraulically fit on the shaft (8) and secured by a locking ring. During the experiment three different overhung configurations W1, W2 and W3 were studied.

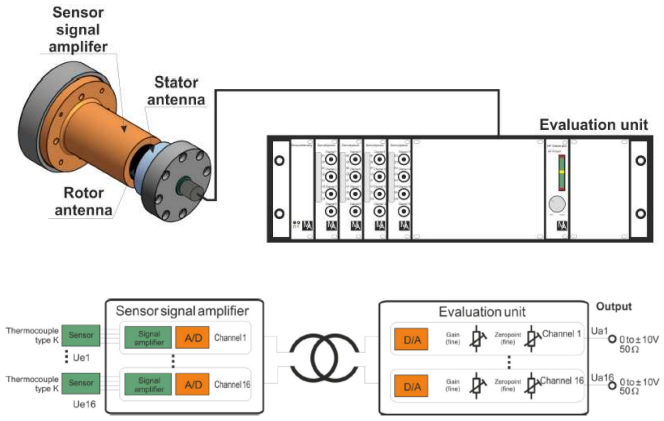

Figure 5: Telemetry Details and Block Diagram

In Table 1 for each configuration the ratio between the equivalent overhung (W_g) and rotor weight (W_r) has been reported for both shaft end sections. The rotor non-drive end overhung was designed to be predominant with respect to the drive-end so to enhance the effect of thermal bow coming from the instrumented journal section. The rotor thermal instability was than mainly driven by the non-drive end bearing that always showed more pronounced synchronous vibration growth.

Configuration W3 corresponds to the case with minimum overhung weight, more precisely to the configuration with no idling adaptor mounted on the shaft. Configuration W1 instead considers the heaviest idling adaptor.

Only the non-drive end journal was instrumented with thermocouples.

Table 1: Rotor configuration

Configuration	W_g/Wr_g [%] Non drive End Side	W_g/Wr_g [%] Drive End Side
W1	12.4	5.4
W2	8.40	5.5
W3	7.30	5.7

LINEAR STABILITY APPROACH

A commonly used strategy to approach stability problems is to assume that linear relationships could be derived among the fundamental physical quantities governing the phenomena. As described by Murphy and Lorenz (Murphy 2009), complex linear influence matrices can be derived in order to link with each other the rotor vibration (V), the imbalance (U) and the rotor thermal gradient (T) as described in Equation 1.

$$\begin{cases} \vec{V} = A\vec{U} \\ \vec{T_{ss}} = B\vec{V} \\ \vec{U} = \vec{U_0} + C\vec{T} \end{cases} \quad \mathbf{1}$$

In Equation 1 U_0 is the initial rotor residual imbalance vector while A, B and C are the complex influence matrices that define the system sensitivity to bearing vibration, rotor thermal gradient and thermal unbalance. During the shaft motion, the rotor thermal gradient dynamics can be also expressed in terms of thermal damping and stiffening as in Equation 2, where D and E are the thermal damping and stiffness complex matrices.

$$D\dot{\vec{T}} + E(\vec{T} - \vec{T_{ss}}) = 0 \quad \mathbf{2}$$

Substituting the vector relations of Equation 1 into Equation 2 it is possible to obtain the final form of the system.

$$\tau\dot{\vec{T}} + (\mathrm{I} - BAC)\vec{T} = BA\vec{U_0} \qquad \tau = E^{-1}D \quad \mathbf{3}$$

where τ is the real non-negative matrix of the thermal time constants of the problem. Equation 3 admits solutions in the form reported in Equation 4:

$$\begin{cases} \vec{T}(t) = \vec{T}e^{st} \\ s = \left(\vec{B}\vec{A}\vec{C} - 1\right)\tau^{-1} \end{cases} \quad \mathbf{4}$$

In order to have a stable solution, a non-negative value for

the eigenvalues s is required, i.e. $\mathrm{Re}\left(\vec{B}\vec{A}\vec{C}\right) \leq 1$. The linear stability approach is formulated in the time domain but in order to compute stability just an accurate knowledge of the sensitivity matrices in terms of both amplitudes and phases is needed.

Among these matrices, the determination of *B* appears to be the most challenging task because predicting such an influent coefficient matrix involves solving a multi-physics problem where fluid lubrication, heat transfer phenomena and rotor dynamics combine in a very complex fashion. Aiming at simplifying such a task, along with a reasonable computational cost Murphy and Lorenz (Murphy 2009, Lorenz 2011) suggested a calculation method for the *B* elements amplitude based on the use of a relatively simple steady-state TPJB code. Their calculation method is considered here with some modifications. The main steps needed to obtain a reasonable estimation of *B* follow:

1. The TPJB code is used to evaluate the equilibrium position of the bearing for given values of speed and supported load;
2. The orbit is discretized to get at each position the film thicknesses seen by the journal, assuming the pads fixed at the equilibrium configuration. Differently from Murphy, the TPJB code is not solved at each orbital position leading also to a computational saving;
3. A simplified energy equation is used to calculate shaft temperature field at each orbit position. Temperature profiles are considered dependent only on the evaluated film thicknesses and oil feeding temperature;
4. Temperatures and film thickness around the shaft are clocked and averaged to find the corresponding mean fields;
5. Mean hot-spot and high-spot positions are evaluated from the averaged fields and both amplitude and phase of B are calculated.

This approach makes the thermal field loosely coupled from the pressure field and dependent to the evaluation of the bearing equilibrium position. The simplified energy equation model is based on what has been suggested by Balbahadur et al. (Balbahadur 2002a) allowing to compute the temperature field based only on the film thickness. In the present work a modified version of the Balbahadur equation is considered since the equivalent viscosity is computed based on the average differential temperature calculated between the pads, making the model more physical. The same energy equation has also been implemented in the in-house TPJB code used for the evaluation of the equilibrium position and a detailed description of that methodology can be found in the following section of the paper. Present algorithm demonstrated to be very efficient even when considering a high number of rotor positions along the orbit and journal surface points.

TPJB Code Description Details

In the present work the TPJB code TILTPAD has been used to find the equilibrium position of the shaft, while the orbit has been obtained from the experimental campaign. TILTPAD is a steady-state thin-film code for tilting pad journal bearing analysis developed at the Department of Industrial Engineering of the University of Florence. It is able to find either the hydrodynamic load on each pad using the shaft equilibrium position and the rotational speed (direct problem) or the shaft equilibrium position once the applied load and the rotational speed are prescribed (inverse problem). The code is an evolution of the FEM code for laminar and iso-viscous plain journal bearing analysis (Martelli 1978) later modified to allow for tilting pad journal bearing calculations (Martelli 1979, Martelli1981). Since detailed descriptions have been referenced, only a few essential information will be given here.

In order to calculate pads' pressure distribution an accurate, high-speed solution is achieved by finite element discretization of the variational formulation of the Reynold's equation, as proposed in the work of Reddi (Reddi 1969). The obtained linear system is solved with the Gauss-Seidel method managing both pressure and oil flow rate as boundary conditions.

The pads' equilibrium problem consists in the evaluation of the tilt angles for which the moment, with respect to the pivot, is zero and the resulting load is correct. The problem can be numerically posed as finding the first zero of the moment, function of the tilt angle, coming from the converging film condition and can be solved by a mixed chord-dichotomic procedure (Martelli 1979). In the first part of the procedure the code scans with prescribed tilt angle steps the whole available tilt angle range in order to define an appropriate interval where moment values at the extremes have an opposite sign. Once the interval has been defined the code uses the method of chords to solve for the root of the equilibrium problem. Stiffness and damping coefficients are also calculated via the "force assembly method" described in (Martelli 1981).

Two different simplified steady-state energy equations have been implemented in the code. The first one is the one suggested by Balbahadur et al. (Balbahadur 2002a) while the second one is an evolution with an improved mixing model to deal with realistic pad inlet temperatures and a temperature-dependent viscosity. The calculation of physically consistent pressure and temperature distributions in the oil-film requires an accurate evaluation of the dynamic viscosity, which is the fundamental parameter in the coupling of the energy and Reynolds' equations. Therefore, instead of using the "equivalent" viscosity suggested by Balbahadur, the local viscosity is calculated by means of the formulation shown in Equation 5.

$$\mu = \mu_0 e^{-\beta(T-T_0)} \quad (5)$$

An iterative procedure is then used between Reynolds and energy equations to obtain convergence both on resulting load and pads temperature.

The basic assumption for the Balbahadur method is that a linear velocity profile can be considered both for the shear strain rate evaluation, involved in the calculation of the dissipation function, and for the evaluation of the convective fluxes. The main consequence of this simplification is to obtain a temperature field for any given film thickness distribution. It has been demonstrated that this Petroff-type simplification gives reasonable accuracy (Cameron 1966). This assumption also allows proposing a mixing model based on an enthalpy and continuity balance, to find pad inlet temperatures.

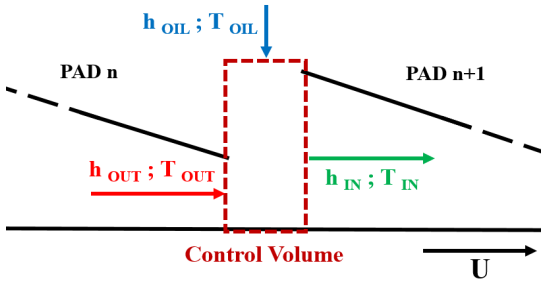

Figure 6: Scheme of mixing model

A control volume between two consecutive pads has been selected and is shown in Figure 6. Since the oil mass-flow is directly related to the film thickness the feeding oil can be evaluated with the difference between the inlet film thickness of "pad n+1" and the outlet film thickness of "pad n". The resulting relation for the evaluation of the inlet temperature of "pad n+1" is shown in Equation 6.

$$T_{IN} = \frac{h_{OUT}}{h_{IN}} T_{OUT} + \frac{h_{IN} - h_{OUT}}{h_{IN}} T_{OIL} \quad (6)$$

The effects of Taylor-Couette vortex flows and transitional flows are also modeled in TILTPAD. A simplified approach proposed by Frene et al. (Frene 1997) has been used for this purpose. It gives a reasonable accuracy until the fully turbulent regime is reached. Under these hypotheses the pressure field seems to be slightly affected by such a model while, on the contrary, dissipative effects are enhanced. The TPJB code has been modified to take into consideration those effects during the evaluation of the local shear stress. Dynamic viscosity is considered a function of the local Reynolds number and the two constants m1 and m2 have been selected from the work of Constantinescu et al. (Constantinescu 1965). The complete set is reported in Equation 7.

$$\begin{cases} \mathrm{Re}_i = \dfrac{\rho U h_{ci}}{\mu_i} \\ \mu_{ti} = \mu_i (1 + m_1 \mathrm{Re}_i^{m_2}) \end{cases} \quad (7)$$

Validation Of The TILTPAD TPJB Code

The validation of the numerical code has been done by means of comparison with both the results obtained using the widely validated commercial code THPAD (Allaire 1980) and using experimental data. Two different rotational speeds, 3000 rpm and 13000 rpm, have been selected since they are representative of the range of operating conditions.

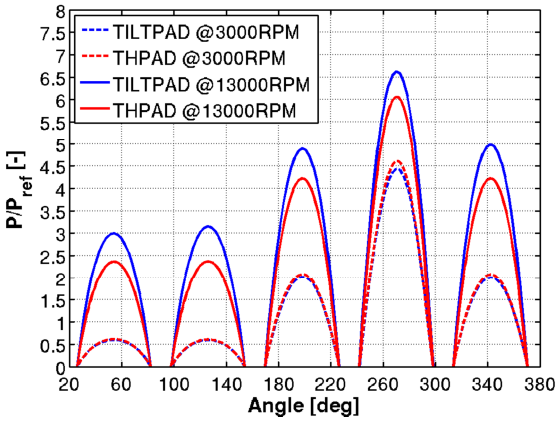

Figure 7: Pressure field: TILTPAD/THPAD comparison

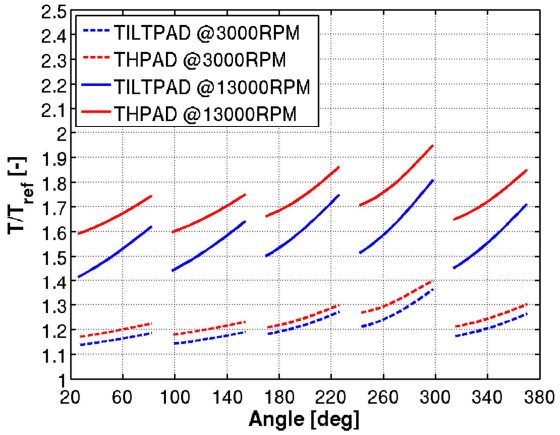

Figure 8: Temperature field: TILTPAD/THPAD comparison

The non-dimensional pressure fields, shown in Figure 7, have been normalized using the bearing unit load as a reference pressure. A very good agreement has been found at the lower rotational speed 3000 rpm, while at 13000 rpm discrepancies up to 33% can be individuated for the pads with lower load. Since pressure and temperature fields are coupled, the reason for these variations can be searched in the temperature fields

shown in Figure 8. Temperature values are non-dimensional with respect to the feeding oil temperature (temperature values have been considered in degree Celsius). It can be observed that the pad inlet temperatures are quite different (-12.5% for the higher rotational speed) and then non-negligible changes in the viscosity field are expected. That difference can be ascribed to the THPAD mixing model (90% of hot oil carry over and a 10% of cold oil injection) that is different from the one implemented in TILTPAD.

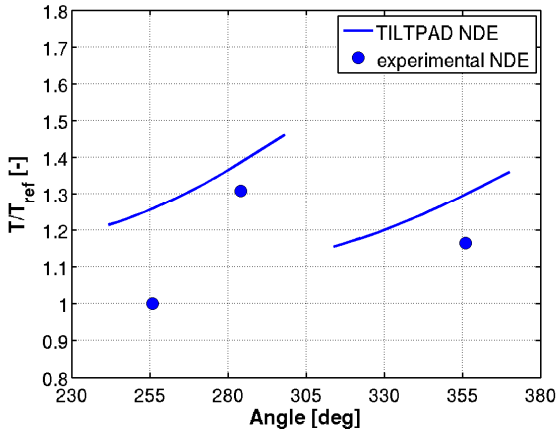

Figure 9: TILTPAD comparison with the experimental temperature on pads

In order to estimate the accuracy of TILTPAD in the evaluation of thermal fields the code has been also compared with available experimental data. Non-dimensional temperature on pads, shown in Figure 9, have been compared for the non-drive end bearing respectively for the most loaded pad and the following one. Results are normalized with respect to the experimental value at 25% of the most loaded pad. Although the trend of the temperature variation of the oil film found is accurate, TILTPAD overestimates temperature levels by a factor of 20% in the worst scenario. It must be underlined that numerical results refer to average oil temperature while probes are positioned few millimeters below pad surface.

Validation of the Linear Method

Both the data by Schmied et al. (Schmied 2008) and by Murphy and Lorenz (Murphy 2009) are used for a preliminary validation of the proposed calculation method for the rotor thermal instability. Figure 10 shows a comparison between the film thickness and temperature mean fields as seen by the shaft of the double overhung turbo-expander supported on TPJB equipped with 5 pads analyzed by Schmied. The phase shift between high- and hot- spot, used to find the B value, is here clearly visible for the 18600 rpm speed case. Here the tangential coordinate rise in the same direction of the shaft rotation showing that the hot-spot lags the high-spot.

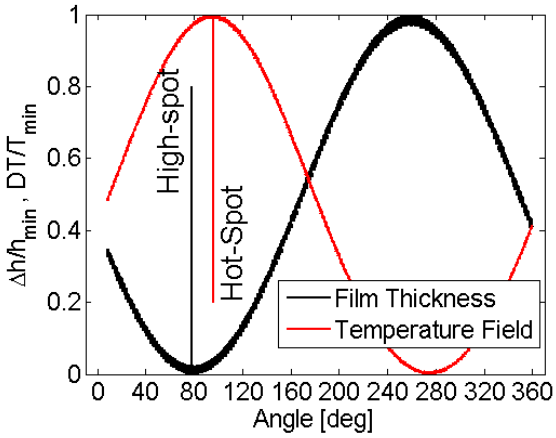

Figure 10: Calculated film height and temperature averaged fields

For that case values of B = 0.18 °C/μm and of phase angle φ_B=18.2° are found, in comparison with B = 0.13 °C/μm calculated by Murphy and the adopted value for the phase angle of φ_B=20° as suggested by de Jongh and Morton (de Jong 1994). It can be concluded that the present algorithm provides results that are in line with the referenced literature.

Further validation of the methodology has been done using the available experimental data. In order to link shaft vibration to rotor differential temperature distribution, an experimental fitting has been derived based on the experimental data (Equation 8)

$$\begin{cases} \Delta T = f_1\left(h, \omega, u, v, lubricant, K_1, K_2\right) \\ \varphi = f_2\left(h, \omega, u, v, lubricant, K_1, K_2\right) \end{cases} \quad \textbf{8}$$

The experimental relations in Equation 8 (f_1 and f_2) allow to extract information on the amplitude of the temperature variation ΔT and on its phase φ and then locate the minimum and the maximum of the temperature distribution in function of the shaft vibration δ_0 and the bearing operating conditions (i.e. lubricant mean fluid film thickness, spinning frequency of the shaft, viscosity, density and heat capacity of the lubricant).

In Figure 11 to Figure 13 the measured values of rotor differential temperature have been compared with the fitted data and the measured vibration trend showing a very good agreement in all tested configurations: W3, W2 and W1. The temperature data have been non-dimentionalized with respect to the maximum measured rotor temperature gradient during the acquisition time. During the recorded time the rotor speed was hold at a fix value. In Figure 11 the data are referring to an instable condition detected during a dwell at a constant speed of 13600 rpm in configuration W3 (see Figure 29 for detailed information).

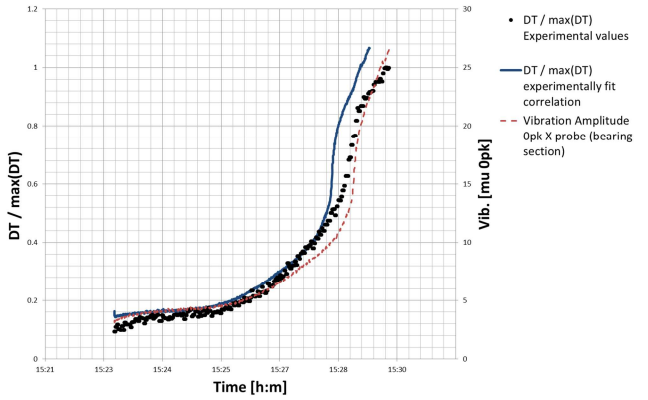

Figure 11: Experimental fit comparison with measured rotor differential temperature data and correlation with the vibration amplitude. Dwell at a constant speed of 13600 rpm, W3 case

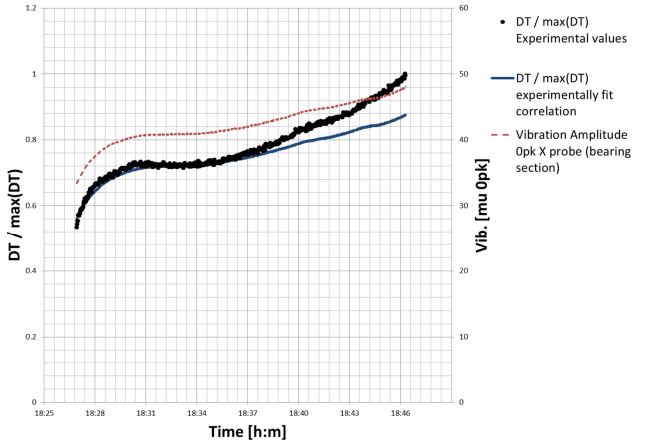

Figure 12: Experimental fit comparison with measured rotor differential temperature data and correlation with the vibration amplitude. Dwell at a constant speed of 10200 rpm, W2 case

In Figure 12 a similar instable condition is reported for the W2 configuration. In this case the threshold of instability reduces from 13600 to 10200 rpm.
In Figure 13 the W1 rotor configuration (higher overhung weight) is reported at 13400 rpm. Despite the high rotor speed, the configuration was stable as it can be seen also by the decreasing trend of the rotor differential temperature.

The experimental correlation can be directly used to compute the experimental B of Equation 1. The term A can be obtained from the rotor response to an overhung imbalance performed with a standard rotordynamic code (see Figure 37).

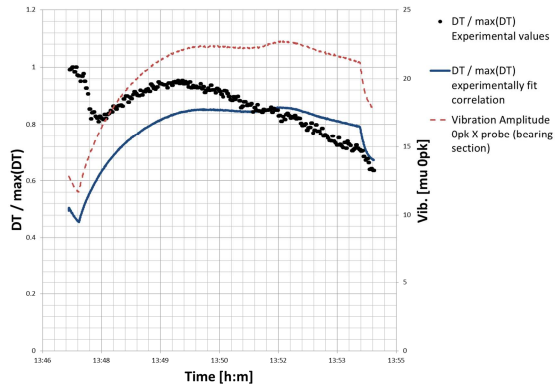

Figure 13: Experimental fit comparison with measured rotor differential temperature data and correlation with the vibration amplitude. Dwell at a constant speed of 13400 rpm, W1 case

In the present work A was only numerically estimated considering the rotor response at the bearing mid line section. The B term instead was experimentally measured. In this case vibration value where taken at probe locations and the temperature gradient was directly measured via telemetry. The C term can be estimated from Equation 9:

$$C = W_g \frac{\alpha L_{jb} L_g}{R_{jb}} \qquad 9$$

In Equation 9 W_g and L_g are the equivalent overhung weight and equivalent overhung length respectively. R_{jb} and L_{jb} represent the bearing radius and axial length respectively and α is the rotor thermal expansion coefficient. The phase of C is always considered to be 180° with respect to the direction of the rotor thermal gradient.

In Figure 14 the BAC term is computed directly from the experimental fitting and using the previously described procedure adapted from Murphy and Lorenz (Murphy 2009) on the basis of the TILTPAD code solution. The graph refers to the W3 configuration and the experimental instability threshold speed is reported as a vertical dashed line. An underestimation of the instability threshold at around 12400 rpm is found. The system was experimentally still stable at 12600 rpm and the first unstable behavior was detected at 13600 rpm. The main difference between the experimentally fit BAC prediction and the computed one is represented by the estimation of the B phase, which affects the computation of the Re(BAC) after the instability threshold. It is important to notice that in both cases the same threshold of instability is predicted. The phase difference of B can be evaluated looking at Figure 15 where the ratio of computed and experimentally fit amplitude of B and phase are reported versus the rotor speed. As can be seen, for the B amplitude ratio, a convergence towards unity appears at

high regimes of rotation. Unfortunately not a similar behavior is shown for the φ_B ratio which estimation is far from the experimental values.

For the overhung configuration W2 the results are shown in Figure 16. Experimentally it is found a shift of the instability threshold towards reduced speed (from 13600 to 10200 rpm). A similar trend is obtained from the linear stability evaluation. . In this case, only the experimental fit predicts a recover of stability. Unfortunately speeds above 10200 rpm were not tested during the experimental campaign. The differences in the evaluation of B for the two models are depicted in Figure 17. Here a similar trend to the W3 configuration is shown. The B predictions became closer to the experiments at higher rotor speeds. The phase of B appears to be again the most difficult parameter to be evaluated.

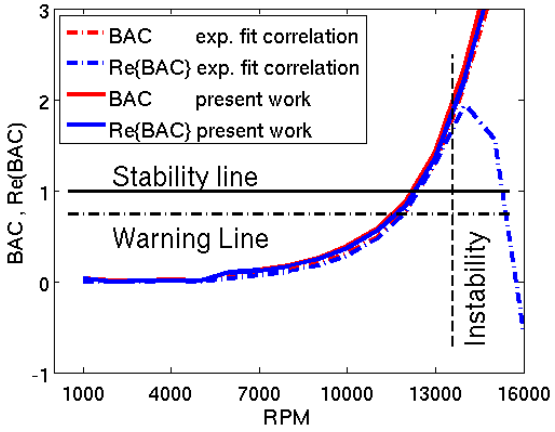

Figure 14: BAC analysis for the W3 configuration rig

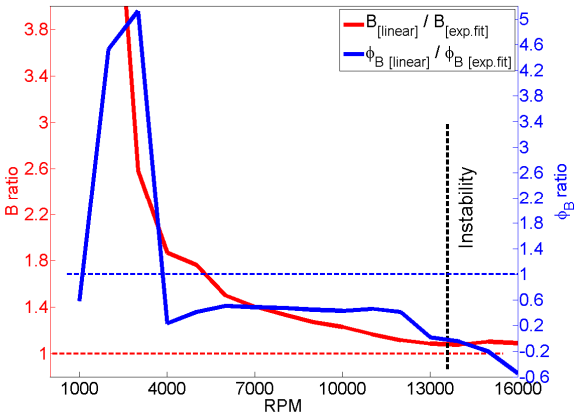

Figure 15: B amplitude and phase comparison for the W3 configuration rig

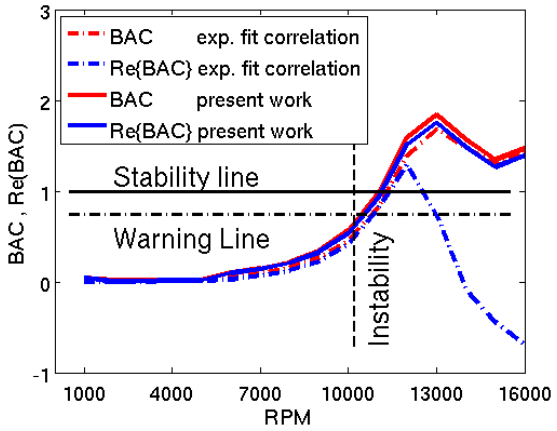

Figure 16: BAC analysis for W2 configuration rig

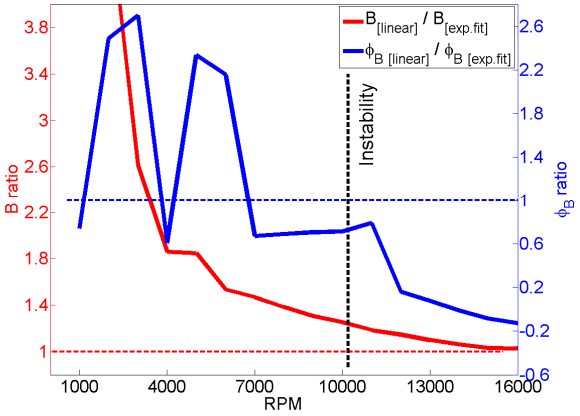

Figure 17: B amplitude and phase comparison for the W2 configuration rig

For the W1 configuration (see results in Figure 18) the stability analysis predicts a marginal instability in the range between 8000 and 10000 rpm and this is the region where a synchronous vibration increase has been experimentally detected (see also the bode plots in Figure 34 and Figure 35). Again a comparison between the Re(BAC) curves gives evidence of discrepancies in the evaluation of B for the linear approach as depicted in Figure 19. In this case the B amplitude ratio approaches unity at the higher speed regimes whereas the phase ratio is far to approach unity in the whole speed range.

In Figure 20 the A term [µm 0-pk/g*mm] is compared for the W1, W2 and W3 rotor configuration. The C term was instead respectively computed as 335, 193 and 144 [g*mm/ ˚C 0-pk].

Based on the shown results, it can be concluded that the linear stability approach can provide quite accurate prediction for the onset of the thermal instability. The implemented methodology results to be quite fast and reliable. This is true even if the linear method is providing very different values for

the phase of B with respect to the experiments.

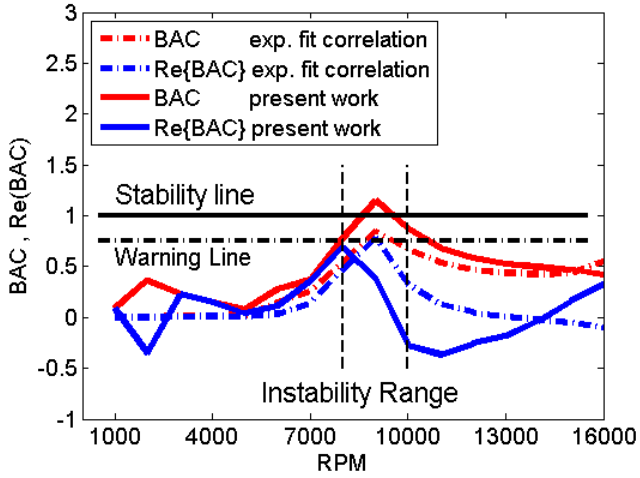

Figure 18: BAC analysis for the W1 configuration rig

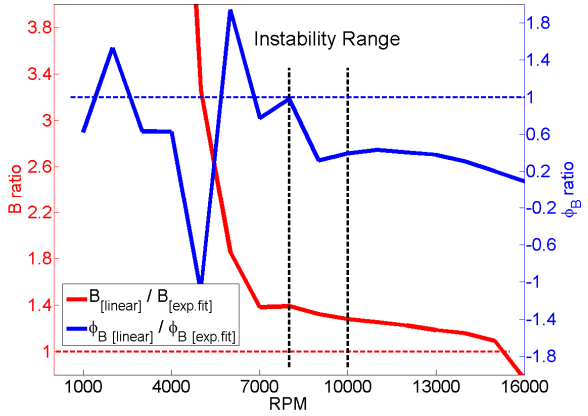

Figure 19: B amplitude and phase comparison for the W1 configuration rig

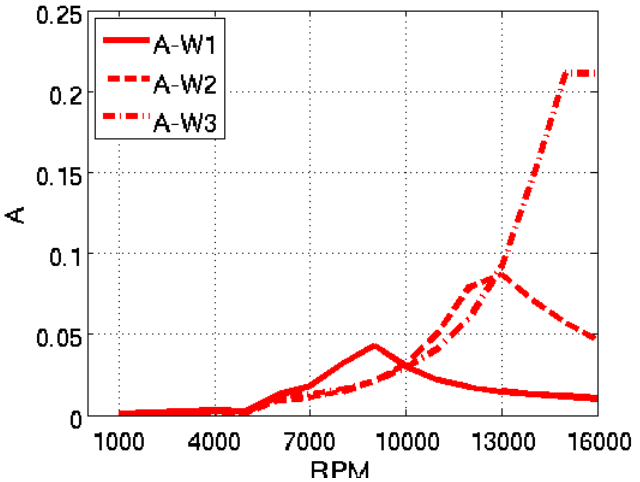

Figure 20: Comparison of computed A term, W1, W2 and W3 case

ITERATIVE METHOD

General Architecture

The model architecture is shown in Figure 21. By assuming a known initial mechanical imbalance u_0, the initial vibration amplitude δ_0 at the bearing section is computed (harmonic analysis) at a given rotor speed (ω). The rotor is considered subjected to the unbalance forces and the bearing stiffness and damping only. By means of the mentioned experimental correlation, the temperature distribution (amplitude ΔT and phase φ) on the surface of the shaft (thermal distribution) is computed using the vibration data calculated in the previous step. A thermo-structural analysis is performed to obtain the distributed forces F_{bf} that produces the thermal deflected configuration of the shaft and this contribution is superimposed to the new harmonic analysis to calculate the new rotor vibrations δ_i. During the calculation loop, depending on the relative phase between thermal distribution and mechanical imbalance, the computed vibrations can converge to a stable solution or grow unbounded depending on the system thermal stability.

The iterative loop stops if the vibration level δ_i exceeds the bearing clearance (cl) and the next rotor speed is analyzed.

Due to the separation of time scales between the fast rotor dynamic response and the slow shaft thermal response, it is assumed that the final stability can be computed considering a succession of quasi-steady states keeping the thermal and dynamic problem segregated.

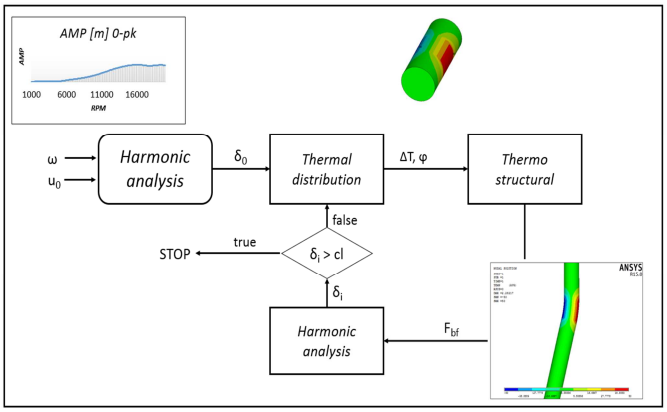

Figure 21: General architecture

The closed loop architecture is fully implemented in Ansys APDL (Ansys Parametric Design Language) so that the rotor design and all related data are standard format inputs valid to model a wide variety of rotor systems. The numerical results, obtained with two different rotor models (a fully 3D and a simplified beam model as shown in Figure 22) have been compared with the experimental data highlighting a good agreement.

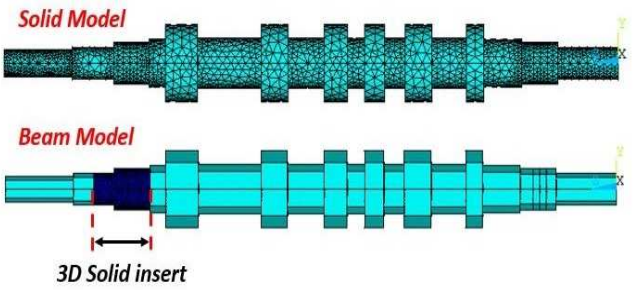

Figure 22: 3d solid model and beam model

The necessity of developing two different models comes from the need to define an accurate and efficient tool able to describe the coupled thermo-rotordynamic phenomenon. The beam model is the simplest formulation able to capture the global behavior of the whole rotor; the solid model instead has the advantage of higher accuracy and to offer the possibility of studying the effect of thermal heat exchange in the whole shaft surface sections if needed.

In the beam model, only the non-drive end bearing section is represented as a 3D solid insert: this allows to describe the temperature distribution on the shaft surface at the instrumented section without further simplification.

All three different overhung configurations W1, W2 and W3 are considered in the following of the paper.

Solid and Beam Rotor Modeling

Due to the high support stiffness only bearings and rotor were modeled. No interactions between supports and bearings have been considered.

The solid model completely represents the rotor exploiting the capability of 3D solid elements, while a reduced formulation of the previous one makes use of beam elements and lumped masses to describe the rotor and a solid 3D insert to calculate the thermal behavior at the instrumented (non-drive end) section.

The mechanical model of the bearing is a classical spring damper element (see Equation 10) where C and K matrices depend on the rotating velocity of the shaft ω:

$$F_i^{BRG} = \begin{Bmatrix} F_x \\ F_y \\ F_z \end{Bmatrix} = \begin{bmatrix} C_{brg\_xx}(\omega) & C_{brg\_xy}(\omega) & 0 \\ C_{brg\_yx}(\omega) & C_{brg\_yy}(\omega) & 0 \\ 0 & 0 & C_{brg\_zz}(\omega) \end{bmatrix} \dot{q}_i + \begin{bmatrix} K_{brg\_xx}(\omega) & K_{brg\_xy}(\omega) & 0 \\ K_{brg\_yx}(\omega) & K_{brg\_yy}(\omega) & 0 \\ 0 & 0 & K_{brg\_zz}(\omega) \end{bmatrix} q_i = C^{BRG}\dot{q}_i + K^{BRG} q_i . \quad \textbf{10}$$

As the model axis is placed along the Z direction, the F_x and F_y components represent the radial bearing reactions while F_z represents the axial component. F_i^{BRG} correspond to the reaction forces vector associated the i-th bearing and q_i represents the displacement vector.

The solid model consists of different coaxial cylindrical sections parametrically generated on the basis of the real rotor dimensions. The rotor dimensions are input through a standard input file that contains the information of the rotor cross section. The built volume is meshed through tetrahedral elements (see Figure 22). Rotor asymmetric heating is prescribed at the rotor/bearing interface nodes (see Figure 23).

The beam model consists of 3D beam elements (2 nodes, 6 DOFs for each node). The different idling adaptors are modeled as lumped masses.

The thermal distribution and all the related forces produced by the shaft bow are imposed over the 3D solid insert (see Figure 22) and the thermal boundary conditions are imposed on the nodes of the rotor/bearing section directly at the 3D insert outer surface.

Only the thermal effect on the non-drive end bearing is considered as it was found to be the main driver for instability.

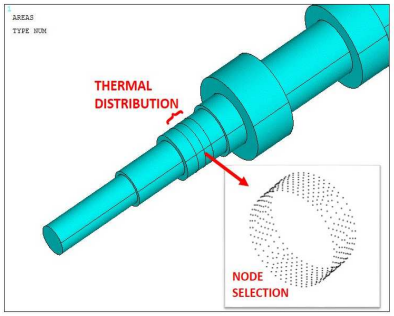

Figure 23: Node selection

The Loop

The first step (harmonic analysis, step 0 of Figure 21) is to model the system through the rotordynamic governing equation:

$$M\ddot{q} + (C + \Omega G)\dot{q} + Kq = F^{BRG} + F^{ext} \quad \textbf{11}$$

In Equation 11 M, C and G represent respectively the mass, the damping and the gyroscopic finite element matrices, while q is the displacements vector, F^{BRG} represents the bearings reaction forces and F^{ext} any external generic loading conditions (Ex. the imposed imbalance u_0 Figure 21). In the frequency domain, considering harmonic displacements, Equation 11 becomes:

$$\left[M\omega^2+i\left(C+C^{BRG}+\Omega G\right)\omega+\left(K+K^{BRG}\right)\right]\delta_0 e^{i\omega t}=F_{ext}e^{i\omega t} \qquad \mathbf{12}$$

where C^{BRG} and K^{BRG} represent the damping and stiffness matrices coming from Equation 10. From the solution of Equation 12 the rotor vibration at bearing location can be determined.

In order to link shaft vibration to rotor differential temperature distribution the already mentioned experimental fitting:

$$\Delta T = f_1\left(h,\omega,u,v,lubricant,K_1,K_2\right)$$
$$\varphi = f_2\left(h,\omega,u,v,lubricant,K_1,K_2\right)$$

has been used. To compute rotor bowing the thermal problem (thermo-structural analysis Figure 21) needs to be solved. The general heat conduction equation in a cylindrical coordinate system (r, φ, z) can be expressed as:

$$\frac{\partial^2 T}{\partial r^2}+\frac{1}{r}\frac{\partial T}{\partial r}+\frac{1}{r^2}\frac{\partial^2 T}{\partial \phi^2}+\frac{\partial^2 T}{\partial z^2}=\frac{c\rho}{k}\frac{\partial T}{\partial t} \qquad \mathbf{13}$$

In a quasi-steady formulation it is possible to neglect the thermal transients (right hand side of Equation 13) and obtain the steady state shaft thermal solution imposing a sinusoidal thermal distribution on the rotor surface. In Figure 24 and Figure 25 the typical hot-spot cold spot temperature distribution and FEA solution is plotted.

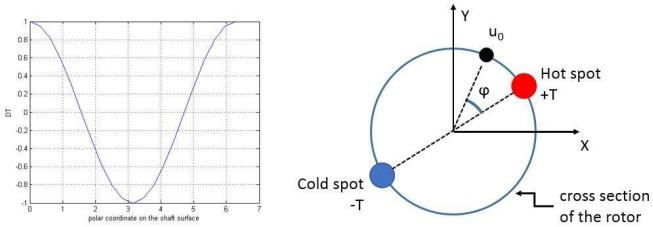

Figure 24: Cross section temperature distribution.

Thanks to the experimental correlation it is possible to link the dynamic response of the rotor (δ_0) to the thermal boundary condition (ΔT, φ) of the rotor heat conduction problem and the result of the thermal analysis is imported into the mechanical model to evaluate the bow effect.

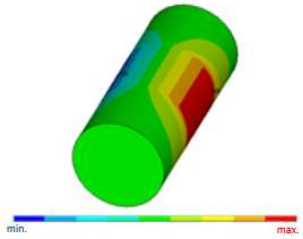

Figure 25: Temperature distribution on the solid element

The thermo-elastic analysis performed at each step of the model (Figure 21) considers the following equation to find the link between deformation and temperature

$$\varepsilon = E^{-1}\sigma+\alpha\Delta T \qquad \mathbf{14}$$

where α is the thermal expansion coefficient, ΔT represents the differential temperature (ΔT=T - T_{ref}, where T_{ref} was set to ambient temperature), E represents the elasticity matrix:

$$\left[E\right]^{-1}=\begin{bmatrix} 1/E_x & -\nu_{xy}/E_x & -\nu_{xz}/E_x & 0 & 0 & 0 \\ -\nu_{yx}/E_y & 1/E_y & -\nu_{yz}/E_y & 0 & 0 & 0 \\ -\nu_{zx}/E_z & -\nu_{zy}/E_z & 1/E_z & 0 & 0 & 0 \\ 0 & 0 & 0 & 1/G_{xy} & 0 & 0 \\ 0 & 0 & 0 & 0 & 1/G_{yz} & 0 \\ 0 & 0 & 0 & 0 & 0 & 1/G_{xz} \end{bmatrix} \qquad \mathbf{15}$$

In particular under the hypothesis of isotropic material with temperature independent coefficient, it is possible to simplify the characterization of the material considering one single value for the Young's modulus E, the Poisson's ratio ν, the shear modulus G, and thermal expansion α.

The rotor bowing is computed and the consequent rotor imbalance is applied in the harmonic analysis (Equation 16) as an equivalent body force F_{bf}:

$$\left[M\omega^2+i\left(\bar{C}+\Omega G\right)\omega+\bar{K}\right]\delta_0 e^{i\omega t}=F_{ext}e^{i\omega t}+F_{bf}e^{i\omega t} \qquad \mathbf{16}$$

In Equation 16, $\bar{C}$ and $\bar{K}$ represent the damping and the stiffness matrices of the system that includes the bearings contribute, while F_{ext} corresponds to the external loads (the mechanical imbalance u_0).

The displacement results of this coupled thermo-structural harmonic response represent the input of the following step of the procedure (δ_i in Figure 21). A new thermal distribution is computed and the loop is iterated till a converging or diverging behavior is obtained (see Figure 26).

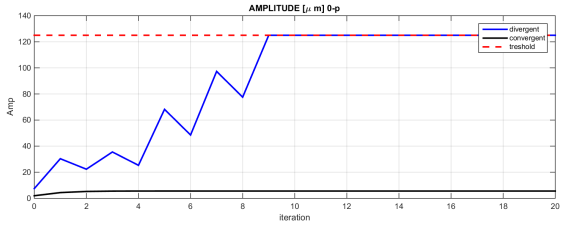

Figure 26: Example of diverging and converging loop solutions

ITERATIVE MODEL COMPARISON WITH EXPERIMENTAL RESULTS

In Figure 27 the response to unbalance of the beam model considering an unbalance of 0.00026 [kg*m] at mid bearing span is reported for the W3 configuration. The results show a first critical speed at 5000 rpm which compare quite well with the experimental data.

In Figure 28 the measured vibrations at rotor mid span have been reported during a ramp up at 10200 rpm and successive coast down. The presence of the first critical speed at 5000 rpm is evident. In Figure 29 a stepped ramp in configuration W3 is reported. Only the X vibration probe is reported at non-drive end bearing location.

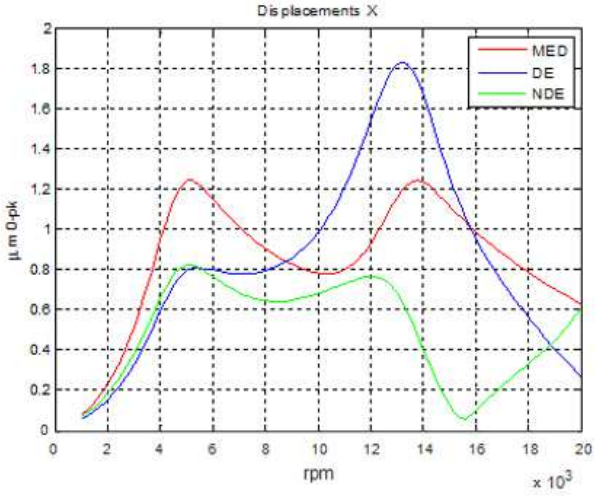

Figure 27: Unbalance response: beam model

During the stepped ramp the rotor speed was hold at 8200, 9200, 10200, 12600 and 13600 rpm for roughly 5 minutes. The rotor vibrations were stable for all speeds with the exception of the case at 13600 rpm where the vibrations increased from 10 μm pp. up to 60 μm pp with a continuous phase change typical of rotor thermal instability.

In Figure 29 and in Figure 30 the iterative model results for the beam and solid models, W3 configuration, were reported respectively. For each rotational speed (Y axis) the zero-peek vibration (expressed in μm) has been reported at each code iteration (X axis) with different colors. Both models seem to predict a threshold of instability right above 12600 rpm in line with the experimental data. Furthermore, the beam and solid models show practically identical results, both in terms of the instability threshold and in terms of the amplitude vibrations. For this reason, the results of the beam model only will be showed hereinafter. The vibration level in the figure was saturated above 120 μm 0-pk.

In Figure 32 a test stepped ramp in configuration W2 is reported. The speed was kept fix at 8200, 10200, 11200 and 11400 rpm. The rotor vibrations were stable at 8200 and 10200 rpm. At 8200 rpm the vibrations were practically constant whereas at 10200 the vibrations stabilized with a 10μm pp vibration increase.

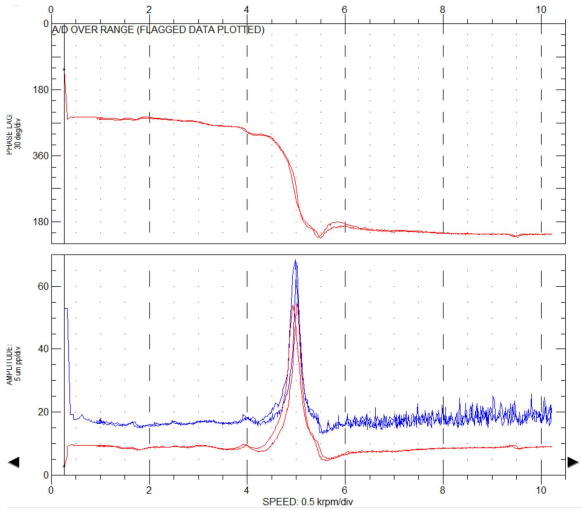

Figure 28: Ramp up and down: mid span X vibration probe

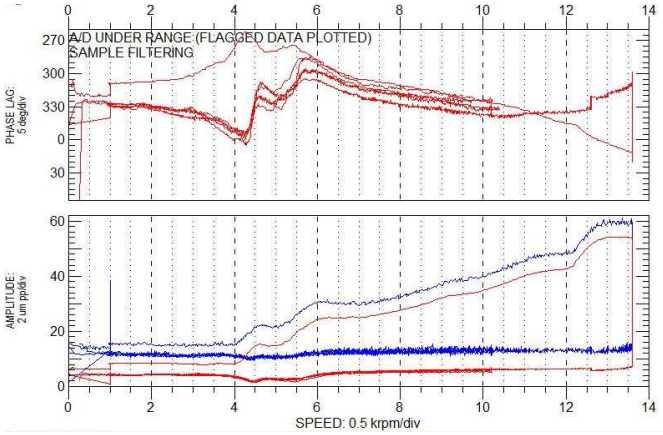

Figure 29: Configuration W3. Stepped ramp, X vibration probe non-drive end bearing

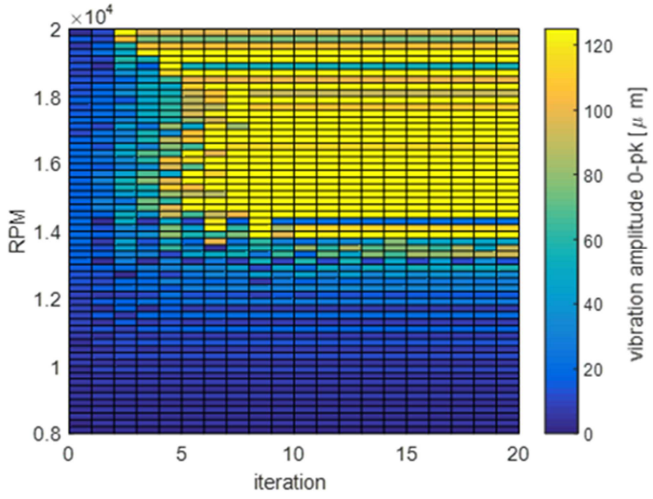

Figure 30: Iterative beam model, configuration W3

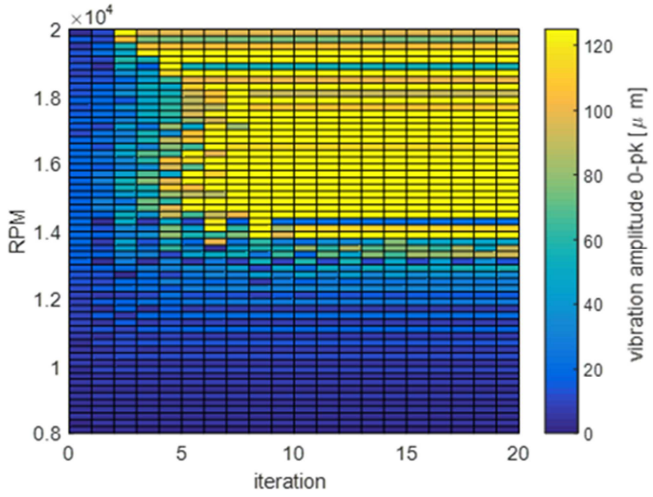

Figure 31: Iterative solid model, configuration W3

At 11200 rpm a small oscillation of vibration amplitude was recorded and at 11400 rpm the vibrations started to grow unbounded. During the ramp down a stop was performed at 10200 rpm with no significative phase and vibration change and at 8200 rpm with a vibration decrease down to the ramp up levels. A hysteresis loop was than evident between 8200 and 11400 rpm also very typical of rotor thermal instability (see de Jongh 1994). In Figure 33 the iterative results of both the solid and beam model have been reported for the case W2. The threshold speed for rotor instability seems to be again very well predicted around 11400 rpm. Between 10000 and 11000 rpm the rotor seems to stabilize at higher level of vibration with respect to their initial value. This was also in line with the experimental rotor behavior in time. As expected the threshold of instability decreased from case W3 to W2 passing from 13600 rpm to 11400 rpm. This can be explained with the increased overhung weight and hence increased sensitivity to rotor bowing.

In Figure 34 the bode plot relative to the configuration W1 is reported. Despite the high level of vibrations no unstable conditions were detected during the speed hold at 10600, 11200, 12200 and 13200 rpm. This was unexpected considering the increase of overhung weight from configuration W2 to W1.

During the speed hold at 10000 rpm instead a bounded vibration increase was recorded whereas for the dwell at

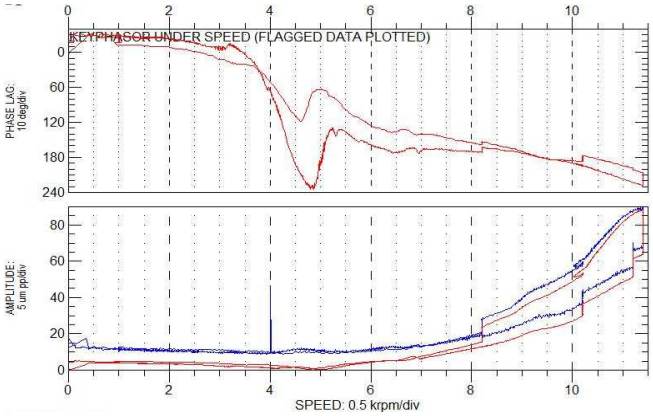

Figure 32 -- Configuration W2. Stepped ramp, x vibration probe, non-drive end bearing.

higher speed a stabilization towards a lower vibration level was experienced. Another rotor run in the same W1 configuration is reported in Figure 35 with speed hold at 13500 and 8000 rpm. Also in these cases the rotor vibrations were bounded showing only a drift of vibration towards higher levels at 8000 rpm.

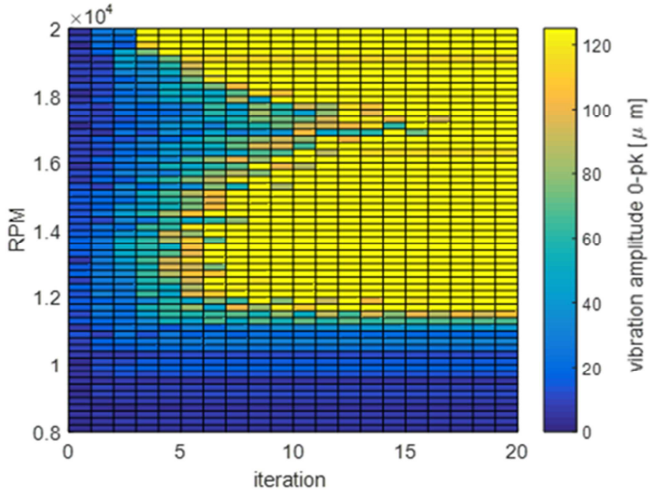

Figure 33: Iterative beam model, configuration W2

The iterative model was able to capture the unexpected stable behavior of the W1 configuration above 11000 rpm. In Figure 36 the results are plot showing rotor instability only close to 8000 rpm and a recovery of stability right above this value.

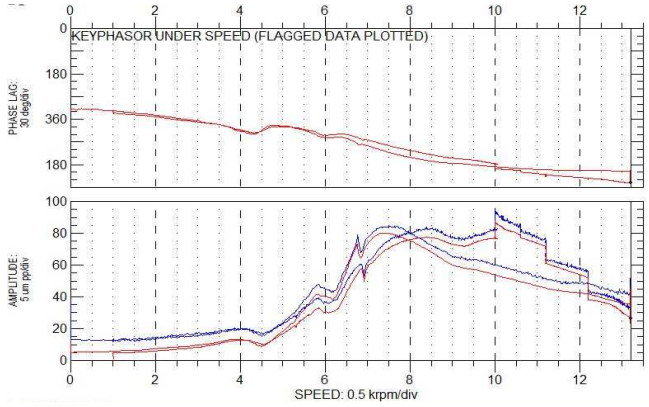

Figure 34: Configuration W1. Stepped ramp, X vibration probe, non-drive end bearing. Speed hold at 10000, 10600, 11200, 12200 and 13200 rpm

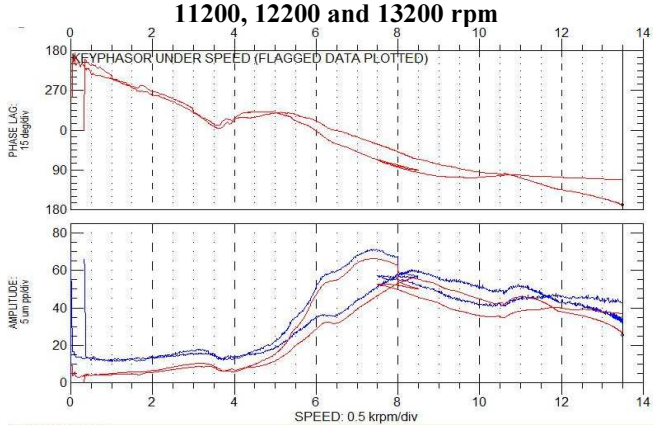

Figure 35: Configuration W1. Stepped ramp, X vibration probe, non-drive end bearing. Speed hold at 13600 and 8000 rpm

In the range between 9000-10000 rpm the model showed stability at higher value of vibration compared to the first iteration. This shows clearly that as in the experiments, in that speed range, the system equilibrium is affected by the thermal unbalance. An advantage of the iterative method on the classical linear stability assessment is that the iterative method is not only capable to predict the system stability but also to evaluate the level of vibration at which the system will converge to a stable solution. This might be critical in order to be sure of not exceeding vibration acceptability levels also in the presence of high rotor thermal unbalance.

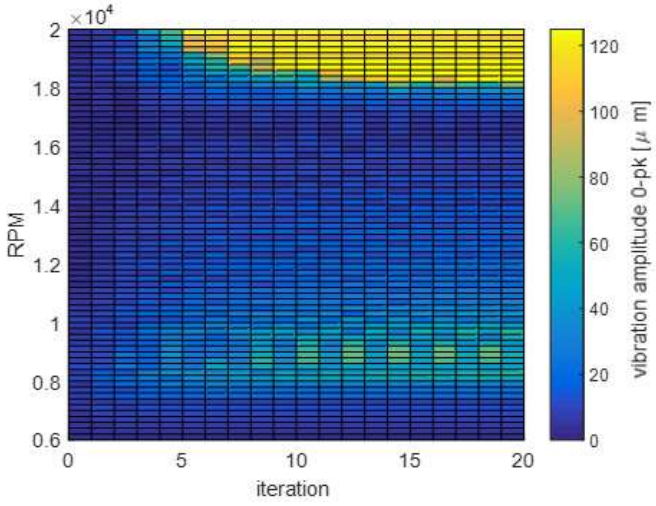

Figure 36: Iterative beam model, configuration W1

In Figure 37 the rotor response to an unbalance placed at the overhung section in the W1, W2 and W3 configurations is reported for both the solid and beam model. The results show a clear shift of the overhung critical speed which can be directly linked to the shift of rotor stability threshold.

In Table 2 the computational time related to the iterative loop of the beam and the solid model rotor description is reported. The beam model seems to require much less computational time with a level of result accuracy comparable with the 3D solid model.

CONCLUSIONS

The stability of a rotor-bearing system is studied following two approaches: a classical linear stability and an original detailed iterative method. The solutions, with a different degree of accuracy are in line with the experimental finding. The linear stability assessment was performed estimating the thermal complex influence matrix B (which links the rotor thermal gradient to the rotor vibration) by means of a steady state tilting pad journal bearing code developed by the University of Florence.

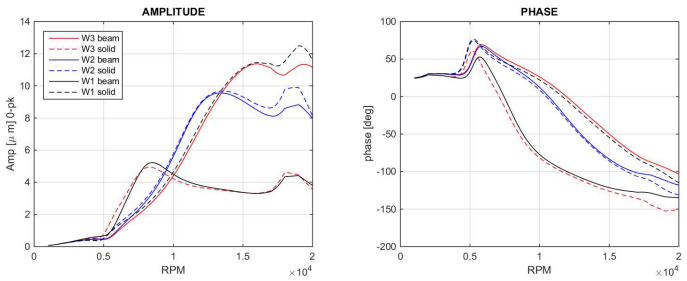

Figure 37: Response to overhung unbalance, model comparison. W1, W2 and W3 configurations.

Table 2: Calculation time

Model	Harmonic response	Thermal Loop
	[hh:mm:ss]	[hh:mm:ss]
Beam	00:00:08	00:00:17
3D Solid	00:00:37	00:01:15

The code estimation seems to differ from the experimental measurements of B mainly for the prediction of the phase. The proposed iterative method instead relied directly on an experimentally fit correlation able to link the thermal rotor gradient to the rotor vibration at bearing section. The detailed model showed good agreement with the experimental results and the capability of estimating not only the overall stability but also the effect of thermal unbalance on the rotor vibration levels in steady conditions. The models were validated against experimental results showing that not always an overhung weight increase is negatively impacting thermal stability. A comparison between detailed 3D model results and simplified linear stability results confirms the reliability of the simple stability method to assess the general system behavior. The determination of the rotor thermal gradient phase remains a critical point and simplified models are shown not to be able to predict this aspect reliably. In this sense more accurate bearing models shall be developed and tested against experimental data giving room for future works.

NOMENCLATURE

W_g	= Equivalent overhung weight	(kg)
W_r	= Rotor weight	(kg)
$\vec{V}$	= Rotor vibration vector	(m)
$\vec{U}$	= Rotor imbalance vector	(kg*m)
$\vec{T}$	= Rotor thermal gradient vector	(K)
$\vec{U_0}$	= Initial rotor imbalance vector	(kg*m)
A	= Sensitivity of vibration to imbalance	(1/kg)
B	= Sensitivity of vibration to temperature	(K/m)
C	= Sensitivity of imbalance to shaft temperature difference	(kg*m/K)
$\vec{T_{ss}}$	= Steady state temperature vector	(K)
D	= Thermal damping	
E	= Thermal stiffness	
T	= Thermal time constant	(s)
s	= Complex eigenvalue	(1/s)
μ	= Dynamic viscosity	(Pa*s)
β	= Thermo-viscosity coefficient	(1/K)
Re	= Reynolds number	
ρ	= Fluid density	(kg/m^3)
U	= Fluid velocity	(m/s)
h_c	= Conventional length	(m)
m_1, m_2	= Constants	
ΔT	= Amplitude of temperature variation	
φ	= Phase of temperature variation	(deg)
h	= Fluid film thickness	(m)
ω	= Rotor angular velocity	(rad/s)
u	= Unbalance	(kg*m)
K_1, K_2	= Constants	
L_g	= Equivalent overhung length	(m)
R_b	= Bearing radius	(m)
L_b	= Bearing axial length	(m)
α	= Thermal expansion coefficient	(1/K)
F_{bf}	= Body forces	(N)
F^{BRG}	= Bearing reaction forces	(N)
C^{BRG}	= Bearing damping matrix	(N*s/m)
K^{BRG}	= Bearing stiffness matrix	(N/m)
q	= Displacement vector	(m)
M	= Mass matrix	
C	= Damping matrix	
G	= Gyroscopic matrix	
K	= Stiffness matrix	
δ_0	= Rotor displacements	(m)
F^{ext}	= External forces	(N)
ε	= Strains	(-)
σ	= Stress	(N/m^2)
E	= Elasticity matrix	(N/m^2)
ν	= Poisson's ratio	(-)
G	= Shear modulus	(N/m^2)

REFERENCES

P. E. Allaire J. D. Parsell L. E. Barrett, "a Pad Perturbation Method for Tilting Pad Journal Bearing Dynamic Coefficients" UVA Report No. UVA/643092/MAE81/183, July 1980.

API 684, 2005.American Petroleum Institute (API), API Recommended Practice 684, API Standard Paragraphs Rotordynamic Tutorial: Lateral Critical Speeds, Unbalance Response, Stability, TrainTorsionals, and Rotor Balancing, Second Edition, August 2005.

Balbahadur, A.C. and Kirk, R.G., 2002a, Part I – Theoretical Model for a Synchronous Thermal Instability Operating in Overhung Rotors, @ Proceedings of IFTOMM, Sixth International Conference on Rotor Dynamics, Sydney, Australia.

Balbahadur, A.C. and Kirk, R.G., 2002b, Part II – Case Studies for a Synchronous Thermal Instability Operating in Overhung Rotors, @ Proceedings of IFTOMM, Sixth International Conference on Rotor Dynamics, Sydney, Australia.

J. Bouyer, M. Fillon, On the Significance of Thermal and Deformation Effects on a Plain Journal Bearing Subjected to Severe Operating Conditions, ASME J. Tribol., Vol. 126, No. 4, pp. 819-822, ISSN: 0742-4787, 2004.

D. Brugier, M.T. Pasal, Influence of elastic deformations of turbogenerator tilting pad bearings on the static behavior and on the dynamic coefficients in different designs, ASME J. Tribol., Vol. 111, No. 2 , pp. 364-371, ISSN: 0742-4787, 1989.

Cameron, A., 1966, The Principles of Lubrication, 292. London, UK: Longmans.

Q. Chang, P. Yang, Y. Meng, S. Wen Thermoelastohydrodynamic analysis of the static performance of tilting-pad journal bearings with the Newton-Raphson method, Tribol. Int., Vol. 35, No. 4, pp. 225-234, ISSN: 0301-679X, 2002.

D. W. Childs and R. Saha, A New, Iterative, Synchronous-Response Algorithm for Analyzing the Morton Effect, Journal of Engineering for Gas turbines and Power, Vol. 134, July 2012.

Constantinescu, V.N. and Galetuse, S., 1965, On the Determination of Friction Forces in Turbulent Lubrication, ASLE Trans., Vol. 8 pp. 367.

Dimarogonas, A. D. Newkirk Effect: Thermally Induced Dynamic Instability of High-Speed Rotors, ASME Paper No.73-GT-26. 1973.

Ulf Ericsson. Temperature Distribution in the Oil Film of a Vibrating Tilting-Pad Bearting, Chalmers University of technology, Götebort, Sweden, 1980.

Frene, J., Nicholas, D., Degueurce, B., Berthe, D., Godet, M., Hydrodynamic Lubrication – Bearings and Thrust Bearings, Elsevier, Tribology Series, 33.

R. Gomiciaga and P. S. Keogh, Orbit Induced Journal Temperature Variation in Hydrodynamic Bearings, Journal of Tribology, Vol. 121, pp. 77-84, January 1999.

B. S. Grigorev and A. E. fedorov and J. Schmied, "New Mathematical Model for the Morton Effect Based on the THD analysis", International Conference on Rotordynamics, Milan 2014 IFTOMM.

Hesseborn, B., 1978, "Measurements of Temperature Unsymmetries in Bearing Journal Due to Vibration," Internal Report ABB Sta.

de Jongh, F. M. and Morton, P. G., 1994, The Synchronous Instability of a Compressor Rotor Due to Bearing Journal Differential Heating, @ ASME paper No. 94-GT-35.

De Jongh, F., and P. van der Hoeven, 1998, Application of a Heat Barrier Sleeve to Prevent Synchronous Rotor Instability, 27th, Turbomachinery Symposium Proceedings, pp. 17-26.

Kellenberger, W., 1979.Spiral Vibrations Due to Seal Rings in Turbogenerators.Thermally Induced Interaction Between Rotor and Stator, ASME Paper No. 79-DET-61. Also published in ASME Transactions, Journal of Mechanical Design, 102, January 1980, pp. 177-184.

Keogh P.S. and Morton P. G., 1993, journal bearing differential heating evaluation with influence on the rotor dynamic behavior, Proc. R. Soc. London, A441 pp. 527-548.

Björn Larsson. Heat Flow Induced Alteration of Rotor Response, Linköping University, Thesis No 661, 1997 ISBN 91-7219-132-5 ISSN 0280-7971.

Lorenz, J.A., and Murphy, B.T. 2011, Case study of Morton effect shaft differential heating in a variable-speed rotating electric machine, @Proc. Of GT2011, ASME Turbo Expo, 6-11 June, 2011, Vancouver, British Columbia, Canada Paper No. GT2011-45228.

Martelli, F. and Manfrida G., 1978, Some applications of finite element technique in journal bearing hydrodynamics, @ Int. Conf. on Numerical Methods in Laminar and Turbulent Flow, University College, Swansea

Martelli, F. and Manfrida G., 1979, Dynamic Properties of the Tilting-pad Journal Bearing – A Finite Element Approach, Int. Conference on Limits of Lubrication, Imperial College, London, 1979.

Martelli, F. and Manfrida G., 1981, A new approach to the theoretical calculation of the dynamic coefficients of tilting-pad bearings, @ Wear, Elsevier Sequoia S.A. Lausanne, 70 (1981) 249-258.

Morton, P. G., 1975, "Some Aspects of Thermal Instability in Generators," G.E.C. Internal Report No.S/W40 u 183.

Murphy, B.T. and Lorenz, J.A., 2009, Simplified Morton Effect Analysis for Synchronous Spiral Instability,@Proc. Of PWR2009, ASME Power, 21-23 July, Albuquerque, New Mexico, USA, Paper No. POWER2009-81030.

Newkirk, B. L., 1926. Shaft Rubbing, Mechanical Engineering, 48, pp. 830-832.

Reddi, M.M., 1969, Finite element solution of the incompressible lubrication problem, @ ASME Transactions, Journal of lubrication technology, pp 524-533.

N.F. Rieger, J.F. Crofoot, Vibrations of Rotating Machinery, Part I: Rotor-Bearing Dynamics, The Vibration Institute, Clarendon Hills, Illinois, 1977.

Schmied, J., 1987. Spiral Vibrations of Rotors, Rotating Machinery Dynamics, 2, Proceedings of ASME Design Technology Conference, Boston, Massachusetts.

Schmied, J. S., Pozivil, J., and Walch, J., 2008, "Hot Spots inTurboexpander Bearings: Case History, Stability Analysis, Measurements and Operational Experience." Proceedings of ASME Turbo Expo 2008: Power for Land,Sea and Air, Berlin, Germany, June 9-13, 2008. ASMEPaper Number GT2008-51179.

J. Suh and A. Palazzolo, Three-Dimensional Thermohydrodynamic Morton Effect Simulation Part I: Theoretical Model, J. Tribol. 136(3), 031706 (2014) (14 pages); Paper No: TRIB-13-1151.

ACKNOWLEDGEMENTS

A special thank goes to the Oil&Gas Technical Laboratory (OGTL) support and in particular to Stefano Cioncolini and Alessio Anichini team who supported the authors during the test design and execution. We would like to acknowledge the useful discussions and reviews had with Simone Salvadori, Giovanni Pallini, Andrea Rindi and Prof. Francesco Martelli from the University of Florence, Department of Industrial Engineering.